

Search for Classical Cepheids in Galactic Open Clusters and Calibration of the Period–Wesenheit–Metallicity Relation in the Gaia Bands

HUAJIAN WANG,^{1,2} YE XU,^{1,2} ZEHAO LIN,^{1,2} CHAOJIE HAO,^{1,2} DEJIAN LIU,^{1,2} AND YINGJIE LI¹

¹*Purple Mountain Observatory, Chinese Academy of Sciences, Nanjing 210008, Peoples Republic of China;*
xuye@pmo.ac.cn

²*University of Science and Technology of China, 96 Jinzhai Road, Hefei 230026, Peoples Republic of China*

ABSTRACT

It is beneficial to calibrate the period–Wesenheit–metallicity relation (PWZR) of Delta Cephei stars (DCEPs), i.e., classical Cepheids, using accurate parallaxes of associated open clusters (OCs) from Gaia data release 3 (DR3). To this aim, we obtain a total of 43 OC-DCEPs (including 33 fundamental mode, 9 first overtone mode, and 1 multimode DCEPs.) and calibrate the PWZR as $W_G = (-3.356 \pm 0.033)(\log P - 1) + (-5.947 \pm 0.025) + (-0.285 \pm 0.064)[\text{Fe}/\text{H}]$. The concurrently obtained residual parallax offset in OCs, $zp = -4 \pm 5 \mu\text{as}$, demonstrate the adequacy of the parallax corrections within the magnitude range of OC member stars. By comparing the field DCEPs’ DR3 parallaxes with their photometric parallaxes derived by our PWZR, we estimated the residual parallax offset in field DCEPs as $zp = -15 \pm 3 \mu\text{as}$. Using our PWZR, we estimate the distance modulus of the Large Magellanic Cloud to be 18.482 ± 0.040 mag, which aligns well with the most accurate published value obtained through geometric methods.

Keywords: methods: data analysis — stars: variables: Cepheids — open clusters and associations: general — stars: distances

1. INTRODUCTION

Delta Cephei stars (DCEPs), i.e., classical Cepheids, constitute Population I of Cepheids and are located in the instability strip above the main sequence in color–magnitude diagrams (CMDs; Turner et al. 2006). A DCEP is a youthful, periodic pulsating yellow giant or supergiant that has been around for tens to hundreds of millions of years, with a pulsation period of approximately 1 to 100 days. The period–luminosity relation, also known as Leavitt’s law (Leavitt & Pickering 1912), is a well-known characteristic of DCEPs. Accurate distances derived from the period–luminosity relationship of DCEPs are widely used. For example, DCEPs have been used to study the structure of the Milky Way (e.g., Chen et al. 2019; Skowron et al. 2019), measure the distances to other galaxies (e.g., Freedman et al. 2001; Sandage & Tammann 2006), and serve as a critical step in measuring the Hubble constant H_0 (e.g., Freedman et al. 2011; Riess et al. 2021).

Various reddening effects are produced by the different lines of sight and distances to DCEPs in the Milky Way. The period–Wesenheit relation (PWR) overcomes the limitations of reddening by transforming multiband magnitudes into Wesenheit magnitudes (Madore 1982; Majaess et al. 2008). Traditionally, the PWR of DCEPs is calibrated using the parallaxes of individual stars (e.g., Ripepi et al. 2019; Poggio et al. 2021; Ripepi et al. 2022). However, this method suffers from uncertain residual parallax offset in the Gaia parallaxes of the individual stars (Lindegren et al. 2021). Besides, it is predicted that a variation in metal abundance affects the shape and width of the DCEP instability strip (e.g., Caputo et al. 2000), which consequently affects the coefficients of the PWR (Marconi et al. 2005, 2010; De Somma et al. 2022, and references therein). Limitations in parallax accuracy led to a stagnation in studies of the period–Wesenheit–metallicity relation (PWZR) until the advent of the Gaia mission (Collaboration et al. 2016), which has provided accurate parallaxes for a total of 1.8 billion objects to date, resulting in a large number of works on the PWZR to spring up (e.g., Groenewegen 2018; Ripepi et al. 2019, 2020, 2021; Riess et al. 2021; Breuval et al. 2022; Ripepi et al. 2022; Cruz Reyes & Anderson 2023; Trentin et al. 2024).

An alternative method to calibrating the PWR or PWZR is to use the parallaxes of open clusters (OCs) harboring DECPs. This newly developed method takes advantage of the stars in the OCs all having a similar distance, extinction, age, and metallicity, as well as the fact that the age distribution

of OCs (ranging from several million years to several billion years; Kharchenko et al. 2013) partially overlaps with the age range of DECPs. After parallax corrections (Lindegren et al. 2021, hereafter L21), this method has been proven to eliminate residual parallax offset (Riess et al. 2022; Cruz Reyes & Anderson 2023), resulting in more accurate PWRs and PWZRs (e.g., Breuval et al. 2020; Zhou & Chen 2021; lin et al. 2022; Riess et al. 2022; Cruz Reyes & Anderson 2023). For example, Riess et al. (2022) used 17 OC-DCEPs with Hubble Space Telescope (HST) photometry to calibrate the PWZR in the HST photometric system and determine a precise Hubble constant of $H_0 = 73.01 \pm 0.99$ km s $^{-1}$ Mpc $^{-1}$.

The first OC-DCEP was discovered by Doig (1925), and searches for OC-DECPs have been active in the past decade (Anderson et al. 2013; Chen et al. 2015; Clark et al. 2015; Chen et al. 2017; Lohr et al. 2018; Alonso-Santiago et al. 2020; Breuval et al. 2020; Negueruela et al. 2020; Medina et al. 2021; Zhou & Chen 2021; Hao et al. 2022; lin et al. 2022; Cruz Reyes & Anderson 2023). Recently, there have been new searches for OCs (e.g., Hunt & Reffert 2023) based on Gaia data release 3 (DR3; Collaboration et al. 2023). In this current study, by cross-matching Gaia sources with the 3655 Galactic DCEPs compiled by Pietrukowicz et al. (2021), we assemble a larger sample of OC-DECPs, which allows us to derive more accurate PWZRs.

The structure of this paper is arranged as follows. In Section 2, we introduce our extended OC-DECP sample. In Section 3, we describe the calibration results for the PWZR derived with our samples. In Section 4, we test the reliability of our PWZR on Galactic field DCEPs and Large Magellanic Cloud (LMC) field DCEPs. Finally, in Section 5, we summarize this work.

2. DATA

2.1. Open Clusters

There are a total of 7167 clusters in the Hunt & Reffert (2024) catalog, which covers almost all previously published OCs. Among these 7167 clusters, we only utilize 3530 high-quality OCs, which all identify clear isochrones by network training methods and filter out moving groups by Jacobi radius. The OCs' coordinates, proper motions, and parallaxes were extracted from Hunt & Reffert

(2024). It should be noted that OC parallaxes from Hunt & Reffert (2024) were derived through the maximum likelihood distances, where L21 corrections had been considered. We obtained the OC parallax error $\sigma_{\varpi_{\text{OC}}}$ by the quadrature sum of the statistical uncertainty and the angular covariance¹ defined by Maíz Apellániz et al. (2021).

2.2. Classical Cepheids

Pietrukowicz et al. (2021) compiled a sample of 3,655 DCEPs in the Milky Way. They also supplied the DR3 source_id of each DCEP by applying a matching radius of 0."5. We used their DR3 source_id to match the gaiadr3.gaia_source and extracted the required parameters (e.g., α , δ , ϖ , μ_{α^*} , and μ_{δ}) for each DCEP. To obtain more reliable photometry of DCEPs, we extracted the intensity-averaged magnitudes ($m_{G_{\text{BP}}}$, $m_{G_{\text{RP}}}$, and m_G) from gaiadr3.vari_cepheid² for 3,046 DCEPs.

2.3. Cross match

OC-DCEPs are identified if the following criteria are met: (1) The projected distance between DCEPs and OCs should be less than 25 pc, assuming that the parallaxes of DCEPs are equal to those of OCs. (2) The μ_{α^*} , μ_{δ} , and ϖ of DCEPs should be within 3σ (σ is the standard deviation of OC) of those of OCs. Additionally, an expanded sample is taken into account, in which a few dimensions are slightly higher than 3σ but less than 3.5σ . (3) DCEPs should be located on the instability strip of their host OC's CMD (Turner et al. 2006). After filtering using the above criteria, we obtained 43 OC-DCEPs, whose astrometry and photometry are given in Table B.1. Representative examples of OC-DCEPs and rejected associations are shown in panels (a) and (b) of Figure A.1, respectively. It should be noted that among the 43 OC-DCEPs we obtained, there is an association of U Sgr with the OC IC 4725, but U Sgr is not in gaiadr3.vari_cepheid and is hence not used for PWZR calibration.

3. ANALYSIS

¹ Due to the large number of member stars in an OC, the statistical uncertainty of the OC's parallax will benefit from the \sqrt{N} improvement. However, as the angular covariance of the Gaia parallaxes is much larger (Lindegren et al. 2021;

Maíz Apellániz et al. 2021; Vasiliev & Baumgardt 2021; Zinn 2021), we took into account the angular covariance.

² <https://gea.esac.esa.int/archive/>

Our 43 OC-DCEPs are composed of 33 DCEPs pulsating in the fundamental mode (F-mode), nine pulsating in the first overtone (1O-mode), and one multimode (F1O-mode) pulsator. To establish the PWZR of the DCEPs including the 1O-mode DCEPs, we used the equation $P_F = P_{1O}/(0.716 - 0.027 \log P_{1O})$ (Feast & Catchpole 1997) to obtain their period in the F-mode, where P_F and P_{1O} represent pulsations in the F-mode and 1O-mode, respectively. For that F1O-mode DCEP, we adopted its period in the F-mode.

To obtain the metal abundances of our OC-DCEPs, we matched our OC-DCEPs with Trentin et al. (2024), who compiled 910 DCEPs with literature metal abundances from high-resolution spectroscopy or metal abundances from the Gaia Radial Velocity Spectrometer (see Section 2.2 in Trentin et al. 2024, for details). Finally, we obtained the metal abundances of 40 OC-DCEPs and compiled them in Table B.1.

To calibrate the PWZR in the Gaia bands, we refer to the method in Riess et al. (2022) and Ripepi et al. (2022). The photometric parallax (in milliarcseconds) is defined as:

$$\varpi_{\text{phot}} = 10^{-0.2(w_G - W_G - 10)}, \quad (1)$$

where w_G is the apparent Wesenheit magnitude and can be defined as $w_G = m_G - \lambda \times (m_{G_{\text{BP}}} - m_{G_{\text{RP}}})$. We adopted the empirical result $\lambda = 1.9$ (Ripepi et al. 2019). W_G is the absolute Wesenheit magnitude, which can be defined as:

$$W_G = \alpha(\log P - 1) + \beta + \gamma[\text{Fe/H}]. \quad (2)$$

We used the `optimize.minimize` method from the `Python Scipy` library to minimize the following quantity:

$$\chi^2 = \sum \frac{(\varpi_{\text{OC}} - \varpi_{\text{phot}} + zp)^2}{\sigma^2} = \sum \frac{(\varpi_{\text{OC}} - \varpi_{\text{phot}} + zp)^2}{\sigma_{\varpi_{\text{OC}}}^2 + \sigma_{\varpi_{\text{phot}}}^2}, \quad (3)$$

where zp is the residual parallax offset in OCs. For $\sigma_{\varpi_{\text{phot}}}$, we refer to the definition given in Ripepi et al. (2022): $\sigma_{\varpi_{\text{phot}}} = 0.46 \times \sqrt{\sigma_{w_G}^2 + \sigma_{W_G}^2} \times \varpi_{\text{phot}}$ and σ_{w_G} is calculated by error propagation,

assuming a conservative error of 0.02 mag for the three Gaia bands (G_{BP} , G_{RP} , and G). We adopted a conservative dispersion of 0.1 mag for σ_{W_G} (De Somma et al. 2020).

To ensure the robustness of the fit, we performed 10,000 Monte Carlo simulations, where for each simulation we randomly varied ϖ_{OC} and σ_{w_G} within their errors to obtain the distribution of each coefficient. Each distribution's median and standard deviation are then taken as the best-fitting value of the coefficient and its error, respectively. The fitting results of our PWR and PWZR are shown in the left and right subfigures of Figure 1, respectively. The marginalised posterior distributions of the free parameters in the fitting are shown in Figure C.1.

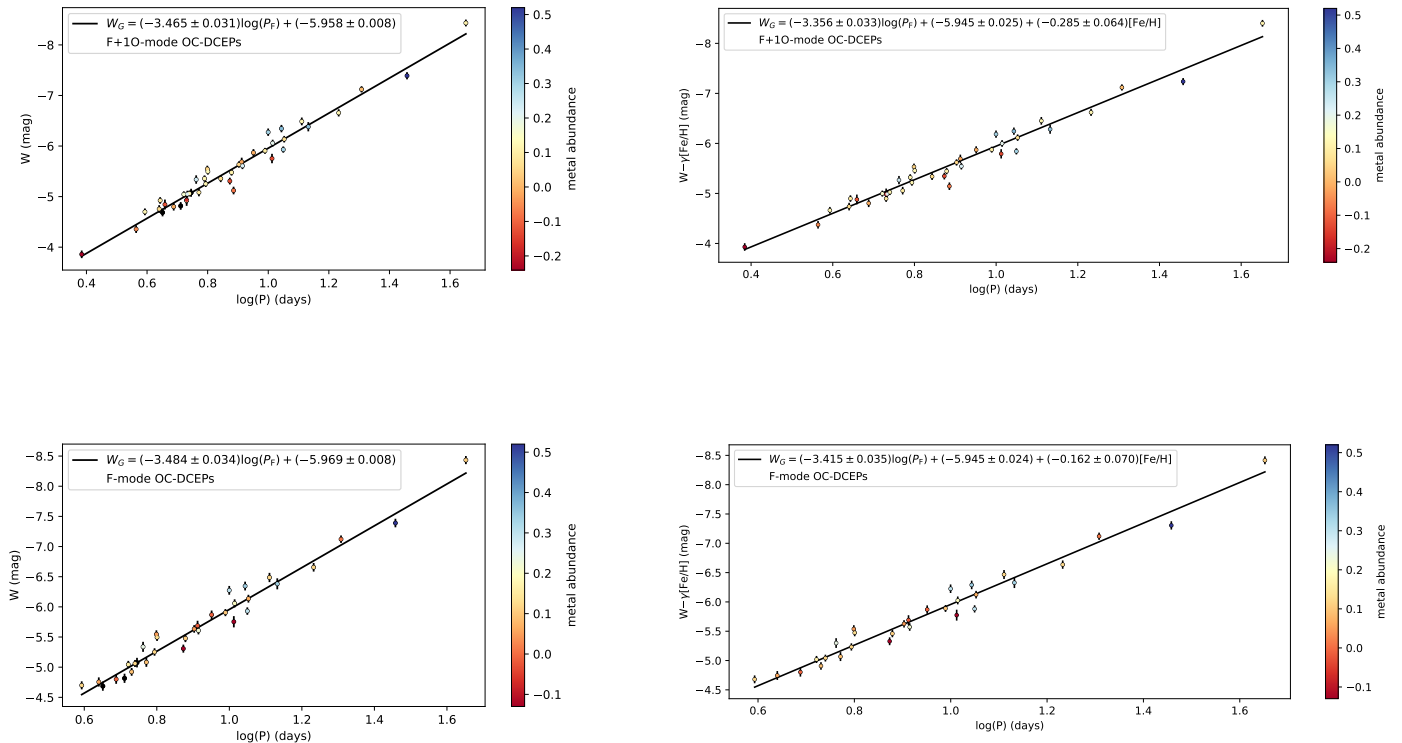


Figure 1. PWR and PWZR fitting results from our OC-DCEPs. The color represents the value of metal abundance. The black dots in the two subfigures on the left are OC-DCEPs without literature metal abundances.

We present our PWZR and compare them with other works in Table 1. The zp of Case 3 and Case 4 in Table 1 are $-4 \pm 5 \mu\text{as}$ and $1 \pm 5 \mu\text{as}$, respectively, which proves the adequacy of L21 corrections

within the magnitude range of OC member stars. As in most works, negative metallicity terms γ are obtained. Specifically, our γ of F-mode OC-DCEPs is -0.162 ± 0.070 , but the γ of F+1O-mode OC-DCEPs is -0.285 ± 0.064 . This is consistent with the conclusions of De Somma et al. (2022), who discovered the γ of ~ -0.1 to ~ -0.2 for the F-mode and ~ -0.1 to ~ -0.3 for the F+1O-mode based on stellar pulsation models. We also found that the absolute value of the γ obtained by the empirical relation of field DCEPs is larger than what we obtained. Our OC-DCEPs have a smaller range of metal abundances, which may explain the smaller absolute value of the γ we obtained. In the future, obtaining more OC-DCEPs with a wider range of metal abundances will help us better constrain the γ .

Cruz Reyes & Anderson (2023) fixed the γ to -0.384 ± 0.051 (Breuval et al. 2022) and then calibrated the PWZR in the Gaia bands using 26 F-mode OC-DCEPs and 225 field DCEPs as $W_G = (-3.242 \pm 0.044) \log(P-1) + (-6.004 \pm 0.019) + (-0.384 \pm 0.051)[\text{Fe}/\text{H}]$. To compare with it, we adopted $\lambda = 1.921$ and fixed the slope α to -3.242 ± 0.044 and the γ to -0.384 ± 0.051 . For our F+1O-mode and F-mode OC-DCEPs, the fitting results of intercept β are -6.008 ± 0.010 mag and -6.046 ± 0.010 mag, respectively. Both fitting results are consistent with Cruz Reyes & Anderson (2023) within 3σ , and the error is smaller.

4. DISCUSSION

4.1. Reliability Testing of PWZR on Galactic Field DCEPs

We chose 758 F+1O-mode Galactic field DCEPs from Trentin et al. (2024) using the following criteria: (1) RUWE < 1.4 ; and (2) $\varpi/\sigma_\varpi > 5$. The OC-DCEPs we obtained and the field DCEPs are plotted together in Figure 2. It can be seen that the linear relation between the two is consistent, and the linear relation of OC-DCEPs is tighter than that of field DCEPs. Then, we applied our F+1O-mode PWZR (i.e., Case 3 in Table 1) on the field DCEPs to derive their photometric parallaxes and parallax offsets, $\Delta\varpi$, between the photometric parallaxes and DR3 parallaxes after L21 corrections

Table 1. Comparison of the Gaia Bands PWZR Obtained in This Work with Other Works

Case	α	β (mag)	γ	zp (μ as)	Mode	μ_{LMC} (mag)	$\Delta\mu_{\text{LMC}}$ (mag)	Sample
This work								
1	-3.465 ± 0.031	-5.958 ± 0.008	–	–	F+1O	18.557 ± 0.014	$0.080(5.7\sigma)$	42 OC-DCEPs
2	-3.484 ± 0.034	-5.969 ± 0.008	–	–	F	18.582 ± 0.016	$0.105(6.6\sigma)$	33 OC-DCEPs
3	-3.356 ± 0.033	-5.947 ± 0.025	-0.285 ± 0.064	-4 ± 5	F+1O	18.482 ± 0.040	$0.005(0.1\sigma)$	39 OC-DCEPs
4	-3.415 ± 0.035	-5.945 ± 0.024	-0.162 ± 0.070	1 ± 5	F	18.520 ± 0.040	$0.043(1.1\sigma)$	30 OC-DCEPs
Ripepi et al. (2022)								
5	-3.176 ± 0.044	-5.988 ± 0.018	-0.520 ± 0.090	–	F+1O	18.513 ± 0.046	$0.036(0.8\sigma)$	435 DCEPs
6	-3.178 ± 0.048	-5.971 ± 0.017	-0.661 ± 0.077	–	F	18.439 ± 0.041	$0.038(0.9\sigma)$	372 DCEPs
Breuval et al. (2022)								
7	-3.338 ± 0.012	-5.959 ± 0.025	-0.384 ± 0.051	–	F	18.474 ± 0.033	$0.003(0.1\sigma)$	2473 DCEPs
Cruz Reyes & Anderson (2023)								
8	-3.242 ± 0.047	-6.004 ± 0.019	-0.384 ± 0.051	$-19 \pm 3^*$	F	18.540 ± 0.034	$0.063(1.9\sigma)$	26 OC-DCEPs + 225 DCEPs
Bhardwaj et al. (2023)								
9	-3.21 ± 0.07	-5.94 ± 0.03	-0.33 ± 0.16	–	F	18.530 ± 0.078	$0.053(0.7\sigma)$	64 DCEPs
Bhardwaj et al. (2024)								
10	-3.54 ± 0.06	-6.21 ± 0.03	-0.47 ± 0.10	–	F+1O	18.577 ± 0.059	$0.100(1.7\sigma)$	60 DCEPs
Trentin et al. (2024)								
11	-3.230 ± 0.041	-5.960 ± 0.018	-0.573 ± 0.066	–	F+1O	18.438 ± 0.038	$0.039(1.0\sigma)$	726 DCEPs
12	-3.245 ± 0.055	-5.917 ± 0.017	-0.745 ± 0.085	–	F	18.323 ± 0.045	$0.154(3.4\sigma)$	478 DCEPs

– means that this parameter does not join in the fitting as a free parameter.

* Residual parallax offset in field DCEPs after L21 corrections.

NOTE— α , β , γ , and zp are the slope, intercept, metallicity term, and residual parallax offset, respectively. μ_{LMC} is the distance modulus of the LMC derived from the PWZR. $\Delta\mu_{\text{LMC}}$ is the difference between μ_{LMC} measured by PWZR and μ_{LMC} measured by Pietrzyński et al. (2019).

(see the distribution of $\Delta\varpi$ in Figure 3). We convoluted this distribution using a Gaussian kernel density estimate (see the orange curve in Figure 3) with a bandwidth chosen according to Silverman (1986), and the $\Delta\varpi$ with the highest probability density (see the red dashed line in Figure 3) is the

estimate of the zp in field DCEPs. To estimate the error of the zp in field DCEPs, we performed 10,000 Monte Carlo simulations, and for each simulation, we randomly varied the coefficients of PWZR (α , β , and γ) within the error to obtain 10,000 estimates of the zp in field DCEPs, and then calculated their standard deviation as the error. Finally, we obtained an estimate of the zp in field DCEPs as $-15 \pm 3 \mu\text{as}$, indicating that L21 overcorrects $15 \mu\text{as}$ for field DCEPs. We show Figure 4 to facilitate comparison of the reported zp in field DCEPs. It can be seen that our estimate of the zp in field DCEPs agrees well with that of Riess et al. (2021), who estimated the zp in field DCEPs as $-14 \pm 6 \mu\text{as}$. Our estimate of the zp in field DCEPs is also consistent with other works (Molinaro et al. 2023; Cruz Reyes & Anderson 2023) within 3σ .

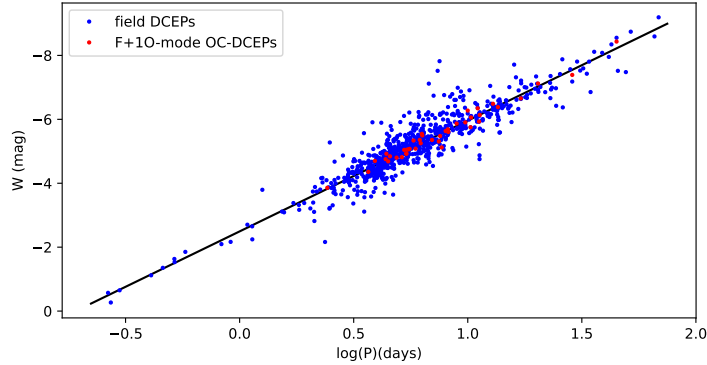


Figure 2. Blue dots are the field DCEPs in Trentin et al. (2024). Red dots are our 42 F+1O-mode OC-DCEPs. The black line is the fitting result of our F+1O-mode PWR.

4.2. Reliability Testing of PWZR on LMC Field DCEPs

The PWZR can be used to measure the distances to LMC field DCEPs and thus infer the distance modulus of LMC (μ_{LMC}). One of the most accurate published distance modulus measurements is $\mu_{\text{LMC}} = 18.477 \pm 0.004$ (statistical error) ± 0.026 (systematic error) mag, obtained from geometric measurements of eclipsing binaries (Pietrzyński et al. 2019). By comparing our PWZR-based distance modulus with the published μ_{LMC} , it is possible to test the reliability of our PWZR on LMC field DCEPs.

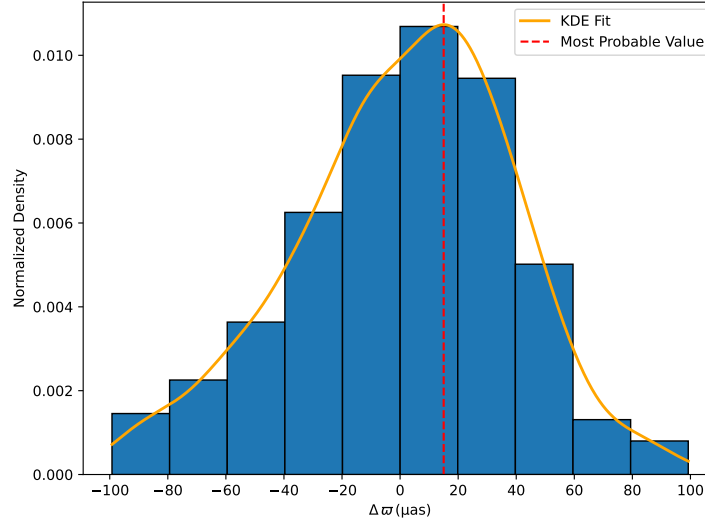


Figure 3. Normalized histogram of parallax offset ($\Delta\varpi$) estimated using our F+1O mode PWZR. The orange curve represents the Gaussian kernel density estimation for this distribution. The red dashed line represents the highest probability density of $\Delta\varpi$.

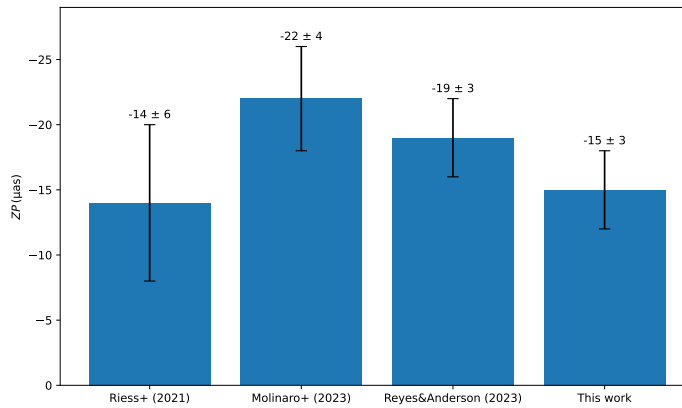


Figure 4. Literature estimates of the zp in field DCEPs.

The DCEPs in the LMC were obtained by the following steps. First, we extracted the α , δ , and P values of 4525 DCEPs in the LMC from the Optical Gravitational Lensing Survey (OGLE) IV survey (Udalski et al. 2018). Second, we matched the α and δ values of each object with gaiadr3.gaia_source to obtain their source_id. Finally, we obtained intensity-averaged magnitudes in the three Gaia bands (G_{BP} , G_{RP} , and G) and calculated the corresponding w_G .

To calculate W_G , we used our PWZR and assumed all the DCEPs in the LMC have the same metal abundance $[\text{Fe}/\text{H}]_{\text{LMC}} = -0.409 \pm 0.003$ dex (Romaniello et al. 2022). The distance modulus of each DCEP was then calculated as $w_G - W_G$, and we took the median value as our estimate of μ_{LMC} . To estimate the error in μ_{LMC} , we performed 10,000 Monte Carlo simulations, and for each simulation we randomly varied the coefficients (α , β , and γ) within their errors to obtain 10,000 medians, and then calculated their standard deviation, σ , as the error of μ_{LMC} .

We list the derived μ_{LMC} in Table 1. $\Delta\mu_{\text{LMC}}$ represents the difference between μ_{LMC} measured by PWZR and μ_{LMC} measured by Pietrzyński et al. (2019). It is evident from a comparison of Table 1 that the LMC’s distance modulus determined by our PWZR is more accurate than found with our PWR, indicating that the latter is indeed affected by the metal abundances of the calibrating DECPs. The $\Delta\mu_{\text{LMC}}$ of Case 3 and Case 4 in Table 1 are 0.005 (0.1σ) and 0.043 (1.1σ), respectively, which are consistent with Pietrzyński et al. (2019) within 3σ , confirming the reliability of our PWZR applied to LMC field DCEPs. We consider Case 3 as the optimal PWZR in this work because it best matches the result derived by Pietrzyński et al. (2019). We also list the μ_{LMC} derived by using other works’ PWZR (i.e., Case 5 to Case 12) in Table 1. All of their μ_{LMC} are consistent with Pietrzyński et al. (2019) within 3σ , with the exception of Case 12, which deviates from Pietrzyński et al. (2019) by 3.4σ .

5. CONCLUSIONS

We obtained a total of 43 OC-DCEPs, which is the largest sample of OC-DCEPs to date. Benefiting from OC’s high-precision parallax, we calibrated the PWZR in the Gaia bands and estimated the zp in OCs simultaneously. We found that the zp in OCs is negligible, demonstrating the adequacy of L21 corrections within the magnitude range of OC member stars. For the metallicity term γ , we

obtained that $\gamma = -0.285 \pm 0.064$ for the F+1O-mode OC-DCEPs and $\gamma = -0.162 \pm 0.070$ for the F-mode OC-DCEPs, which is consistent with the conclusions of De Somma et al. (2022). Applying our F+1O model PWZR on field DCEPs and using a Gaussian kernel density estimate, we found that the $zp = -15 \pm 3 \mu\text{as}$ in field DCEPs, which is in good agreement with Riess et al. (2021). Our best PWZR is $W_G = (-3.356 \pm 0.033) \log(P - 1) + (-5.947 \pm 0.025) + (-0.285 \pm 0.064)[\text{Fe}/\text{H}]$. This PWZR estimates a μ_{LMC} value of 18.482 ± 0.040 mag, which aligns well with the result derived by Pietrzyński et al. (2019) based on the geometric measurements of eclipsing binaries in the LMC. As more OC-DECPs are identified and more precise astrometric data are published in future releases from Gaia, more precise PWZR will likely be obtained.

APPENDIX

A. EXAMPLES OF OC-DCEPS AND REJECTED ASSOCIATIONS

Here, we provide an example of our OC-DCEPs as well as an example of rejected associations in figure A.1. Because DCEPs have left the main sequence and entered the instability strip, they should be brighter than the main sequence member stars.

B. 43 OPEN CLUSTER CEPHEIDS

Here, we present the parameters for 43 OC-DCEPs obtained by us (listed in Table B.1).

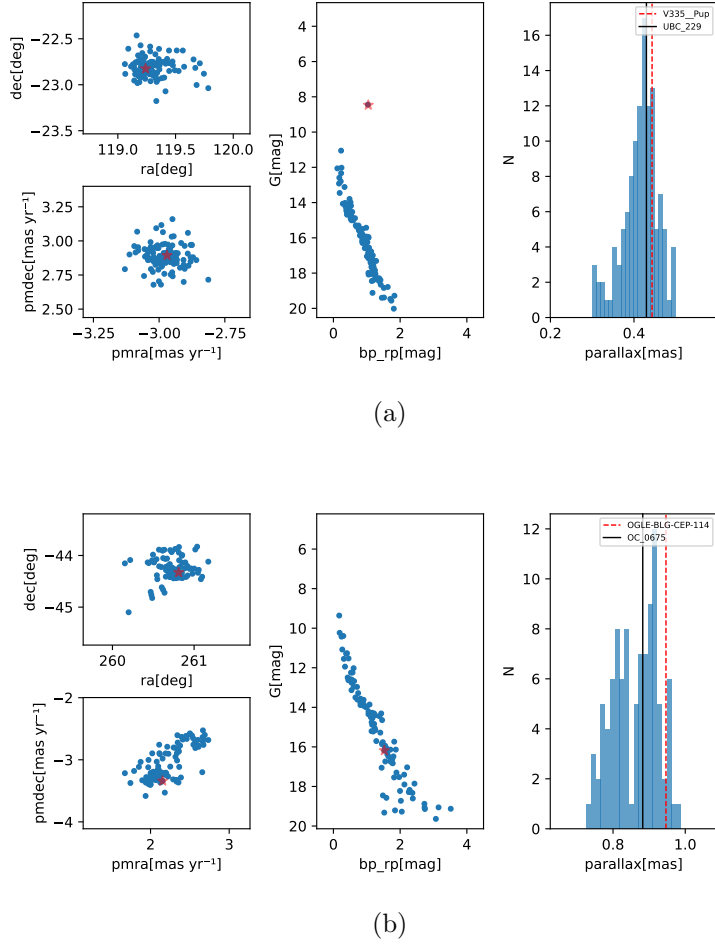


Figure A.1. Examples of the OCs (blue dots) harboring one or more DCEPs (red stars). The upper left, lower left, and middle images of each subfigure show their coordinates (α and δ), proper motions (μ_{α^*} and μ_{δ}) distribution, and the CMD, respectively. The blue histogram on the right shows the parallax distribution of the member stars, where the black solid line represents the mean parallax of the OC and the red dotted line represents the parallax of the DCEP. (a) An example of OC-DCEPs. (b) An example of rejected associations.

Table B.1. Parameters of the 43 Open Cluster Cepheids

Cluster	Cluster parameter						Cepheid parameters												
	α (deg)	δ (deg)	ϖ (mas)	$\sigma_{\varpi_{\text{OC}}}$ (mas)	μ_{α^*} (mas yr $^{-1}$)	μ_{δ} (mas yr $^{-1}$)	N	Sep (pc)	Cepheid	α (deg)	δ (deg)	ϖ (mas)	μ_{α^*} (mas yr $^{-1}$)	μ_{δ} (mas yr $^{-1}$)	w_G (mag)	Mode	P_F (day)	[Fe/H]	Ref
NGC_7790	359.620	61.208	0.320(0.025)	0.007	-3.243(0.059)	-1.726(0.059)	143	21.40	CG---Cas	0.247	60.959	0.296	-3.241	-1.673	7.721	F	4.365	0.06	G18
NGC_7790	359.620	61.208	0.320(0.025)	0.007	-3.243(0.059)	-1.726(0.059)	143	2.18	CE---Cas.B	359.538	61.214	0.333	-3.301	-1.809	7.790	F	4.479		
NGC_7790	359.620	61.208	0.320(0.025)	0.007	-3.243(0.059)	-1.726(0.059)	143	2.14	CE---Cas.A	359.539	61.214	0.332	-3.298	-1.873	7.660	F	5.141		
NGC_7790	359.620	61.208	0.320(0.025)	0.007	-3.243(0.059)	-1.726(0.059)	143	1.39	CF---Cas	359.575	61.221	0.316	-3.240	-1.766	7.675	F	4.875	-0.01	G18
SAL_4	5.905	62.708	0.341(0.033)	0.008	-3.098(0.081)	-0.624(0.057)	71	17.80	V324---Cas	5.630	63.033	0.296	-2.868	-0.588	7.213	IO	7.684	-0.08	R21
NGC_103	6.311	61.326	0.316(0.053)	0.007	-2.815(0.110)	-1.066(0.091)	418	7.77	NO---Cas	6.019	61.342	0.298	-2.828	-1.208	8.144	IO	3.664	-0.06	GRD3
NGC_129	7.590	60.206	0.559(0.044)	0.007	-2.586(0.110)	-1.177(0.108)	561	23.47	V379---Cas	6.650	60.798	0.524	-2.696	-1.313	5.907	IO	6.162	0.12	G18
NGC_129	7.590	60.206	0.559(0.044)	0.007	-2.586(0.110)	-1.177(0.108)	561	1.51	DL---Cas	7.494	60.212	0.580	-2.706	-1.189	5.629	F	8.000	0.05	G18
COIN-Gaia_36	36.341	59.935	0.476(0.042)	0.007	-0.985(0.096)	-0.545(0.091)	183	24.41	GM---Cas	36.736	60.571	0.418	-0.904	-0.383	6.304	F	7.468	-0.13	G18
CWNU_2490	58.992	55.335	0.337(0.043)	0.009	-0.442(0.065)	-0.717(0.088)	30	23.47	MN---Cam	59.374	54.938	0.366	-0.263	-0.645	6.674	F	8.173	-0.02	G18
UBC_1273	74.936	40.821	0.285(0.032)	0.010	-0.380(0.067)	-1.502(0.069)	32	1.08	AN---Aur	74.923	40.836	0.285	-0.427	-1.515	6.974	F	10.289	-0.13	G18
CC_0301	88.378	25.183	0.358(0.061)	0.008	-0.400(0.123)	-1.847(0.146)	100	24.06	J055122+2516.9	87.844	25.281	0.362	0.609	-1.627	8.373	IO	2.423	-0.24	GRD3
FSR_0951	95.544	14.658	0.609(0.038)	0.007	-0.226(0.103)	-0.013(0.101)	221	0.67	RS---Ori	95.555	14.678	0.589	0.196	0.005	5.598	F	7.567	0.11	G18
vdBergh_1	99.273	3.079	0.587(0.062)	0.008	-0.388(0.113)	-0.711(0.112)	86	0.46	CV---Mon	99.270	3.064	0.601	0.349	-0.666	6.236	F	5.379	0.09	G18
UBC_231	115.544	-26.313	0.360(0.033)	0.007	-2.247(0.085)	-2.260(0.097)	98	21.25	WX---Pup	115.496	-25.876	0.387	-2.164	2.559	6.350	F	8.936	-0.01	G18
UBC_1429	118.566	-37.005	0.320(0.026)	0.008	-2.753(0.084)	-3.770(0.112)	58	5.89	V724---Pup	118.438	-36.970	0.318	-2.678	3.857	7.400	F	5.564		
UBC_229	119.253	-22.813	0.430(0.041)	0.008	-2.979(0.057)	-2.885(0.082)	121	0.70	V335---Pup	119.240	-22.825	0.443	-2.970	2.894	6.478	IO	6.969	0.06	G18
Ruprecht_79	145.261	-53.834	0.276(0.043)	0.006	-4.588(0.076)	-3.043(0.084)	316	1.65	CS---Vel	145.293	-53.816	0.272	-4.567	3.131	7.713	F	5.905	0.09	G18
HSC_2354	158.759	-59.631	0.235(0.028)	0.011	-5.495(0.080)	-2.401(0.062)	46	0.64	525451876011884864	158.775	-59.635	0.239	-5.563	2.466	8.214	IO	5.379	-0.18	GRD3
CWNU_175	188.407	-63.515	0.730(0.032)	0.006	-3.901(0.106)	-1.186(0.086)	55	0.87	VW---Cru	188.328	-63.506	0.738	-3.903	-1.134	5.638	F	5.265	0.16	G18
UBC_290	191.742	-59.376	0.644(0.039)	0.007	-5.952(0.106)	-0.213(0.103)	355	7.12	X---Cru	191.593	-59.125	0.654	-5.926	-0.173	5.704	F	6.220	0.12	G18
NGC_5662	218.927	-56.575	1.332(0.050)	0.007	-6.495(0.180)	-7.204(0.186)	439	7.00	V---Cen	218.138	-56.488	1.409	-6.697	-7.068	4.317	F	5.494	0.12	G18
CWNU_19	228.514	-54.536	0.536(0.033)	0.007	-0.780(0.120)	-1.758(0.101)	84	9.21	IQ---Nor	228.206	-54.755	0.535	-0.897	-1.821	5.747	F	8.220	0.22	G18
Thela_3005	242.885	-54.321	0.512(0.018)	0.008	-1.882(0.124)	-3.862(0.112)	97	1.50	QZ---Nor	242.835	-54.534	0.484	-1.896	-3.848	6.403	IO	5.407	0.21	G18
NGC_6067	243.295	-54.232	0.511(0.038)	0.007	-1.961(0.118)	-2.578(0.119)	1149	0.56	V340---Nor	243.322	-54.235	0.491	-2.066	-2.634	5.323	F	11.289	0.07	G18
NGC_6087	244.683	-57.914	1.066(0.054)	0.007	-1.601(0.202)	-2.427(0.163)	360	0.37	S---Nor	244.716	-57.900	1.099	-1.608	-2.136	3.936	F	9.754	0.10	G18
UBC_1558	252.706	-45.414	0.429(0.028)	0.008	-1.319(0.097)	-2.503(0.073)	64	5.87	KQ---Sco	252.911	-45.427	0.472	-1.366	-2.497	4.450	F	28.703	0.52	G18
HSC_2961	267.492	-32.977	0.636(0.032)	0.008	-1.879(0.187)	-1.776(0.185)	51	19.22	RY---Sco	267.718	-33.706	0.764	1.485	-1.388	3.665	F	20.322	0.01	G18
CWNU_1841	272.828	-20.884	0.402(0.016)	0.013	-0.033(0.174)	-1.452(0.125)	41	11.02	YY---Sgr	273.019	-20.704	0.412	0.307	-1.548	5.598	F	13.558	0.33	G18

Table B.1 continued on next page

Table B.1 (*continued*)

Cluster	Cluster parameter						Cepheid parameters											
	α (deg)	δ (deg)	ϖ (mas)	$\sigma_{\varpi_{OC}}$ (mas)	μ_{α^*} (mas yr^{-1})	μ_δ (mas yr^{-1})	N	Sep (pc)	Cepheid	α (deg)	δ (deg)	ϖ (mas)	μ_{α^*} (mas yr^{-1})	μ_δ (mas yr^{-1})	w_G (mag)	Mode	P_F (day)	[Fe/H]
IC_4725	277.942 -19.131 1.551(0.045)	0.007 -1.692(0.188) -6.165(0.218)	725	0.32	U_____Sgr	277.972 -19.125 1.605	-1.795	-6.127	F	6.745	0.14	G18						
NGC_6649	278.359 -10.402 0.510(0.063)	0.007 -0.037(0.131) -0.115(0.133)	728	1.55	V367_Sct	278.397 -10.427 0.473	0.082	-0.273	5.916	F1O	6.293	0.05	G18					
NGC_6664	279.118 -8.206 0.502(0.054)	0.007 -0.099(0.158) -2.593(0.151)	482	1.78	EV____Sct	279.165 -8.185 0.526	-0.209	-2.546	6.575	1O	4.398	0.09	G18					
CWNU_337	279.158 -8.909 0.570(0.034)	0.009 -0.731(0.071) -2.846(0.086)	32	19.72	Y____Sct	279.514 -8.369 0.558	-0.737	-2.878	5.162	F	10.341	0.20	G18					
Trumpler_35	280.747 -4.228 0.374(0.051)	0.008 -0.983(0.090) -2.243(0.107)	257	10.43	TY____Sct	280.533 -4.293 0.371	-1.106	-2.466	5.791	F	11.054	0.34	G18					
Trumpler_35	280.747 -4.228 0.374(0.051)	0.008 -0.983(0.090) -2.243(0.107)	257	7.38	CN____Sct	280.627 -4.331 0.390	-1.042	-2.255	5.862	F	9.994	0.30	G18					
UBC_106	280.492 -5.417 0.440(0.041)	0.007 -1.053(0.099) -1.361(0.115)	664	5.61	CM____Sct	280.612 -5.341 0.444	-1.064	-1.414	7.084	F	3.917	0.12	G18					
NGC_6683	280.566 -6.225 0.328(0.032)	0.008 -0.343(0.067) -2.344(0.063)	83	23.32	Z____Sct	280.739 -5.821 0.357	-0.379	-2.205	5.931	F	12.902	0.12	G18					
UBC_130	298.061 27.449 0.424(0.027)	0.007 -2.107(0.061) -5.876(0.108)	142	6.67	SV____Vul	297.879 27.460 0.402	-2.158	-5.962	3.429	F	44.894	0.11	G18					
UBC_129	299.035 26.445 0.887(0.056)	0.007 -0.984(0.106) -4.369(0.125)	348	6.29	X____Vul	299.369 26.556 0.864	-1.352	-4.247	4.766	F	6.320	0.13	G18					
UBC_135	299.817 33.724 0.267(0.043)	0.007 -3.512(0.069) -6.429(0.099)	163	4.24	GI____Cyg	299.890 33.746 0.273	-3.452	-6.577	7.527	F	5.783	0.24	G18					
Berkeley_84	301.200 33.986 0.393(0.043)	0.008 -2.012(0.070) -5.555(0.096)	103	6.51	CD____Cyg	301.111 34.112 0.394	-1.970	-5.583	5.370	F	17.079	0.12	G18					
vdBerg_130	304.517 39.367 0.536(0.035)	0.006 -3.548(0.293) -5.127(0.165)	162	20.97	V438_-Cyg	304.726 40.064 0.530	-3.324	-4.559	5.193	F	11.210	0.30	G18					
Kronberger_84	323.888 53.514 0.210(0.025)	0.008 -2.920(0.087) -3.032(0.065)	79	0.12	J213533.70+533049.3	323.890 53.514 0.214	-2.878	-3.113	8.541	1O	4.561	-0.12	GDR3					

NOTE—Values in parentheses are standard deviations. N is the number of member stars in the OC. $\sigma_{\varpi_{OC}}$ is the total uncertainty, including the contribution from angular covariance. “Sep” is the distance between the DCEP and OC. w_G is the apparent Wesenheit magnitude in the Gaia bands. “Ref” is the reference for the metallicity of DCEP.

References—G18: Groenewegen (2018); R21: Ripepi et al. (2021); GDR3: Recio-Blanco et al. (2023).

C. THE MARGINALISED POSTERIOR OF DISTRIBUTIONS

REFERENCES

- Alonso-Santiago, J., Negueruela, I., Marco, A., Tabernero, H. M., & Castro, N. 2020, A&A, 644, A136, doi: [10.1051/0004-6361/202038495](https://doi.org/10.1051/0004-6361/202038495)
- Anderson, R. I., Eyer, L., & Mowlavi, N. 2013, Monthly Notices of the Royal Astronomical Society, 434, 2238, doi: [10.1093/mnras/stt1160](https://doi.org/10.1093/mnras/stt1160)
- Bhardwaj, A., Riess, A. G., Catanzaro, G., et al. 2023, ApJL, 955, L13, doi: [10.3847/2041-8213/acf710](https://doi.org/10.3847/2041-8213/acf710)
- Bhardwaj, A., Ripepi, V., Testa, V., et al. 2024, A&A, 683, A234, doi: [10.1051/0004-6361/202348140](https://doi.org/10.1051/0004-6361/202348140)
- Breuval, L., Riess, A. G., Kervella, P., Anderson, R. I., & Romaniello, M. 2022, ApJ, 939, 89, doi: [10.3847/1538-4357/ac97e2](https://doi.org/10.3847/1538-4357/ac97e2)
- Breuval, L., Kervella, P., Anderson, R. I., et al. 2020, Astronomy and Astrophysics, 643, A115, doi: [10.1051/0004-6361/202038633](https://doi.org/10.1051/0004-6361/202038633)
- Caputo, F., Marconi, M., Musella, I., & Santolamazza, P. 2000, A&A, 359, 1059, doi: [10.48550/arXiv.astro-ph/0006228](https://doi.org/10.48550/arXiv.astro-ph/0006228)
- Chen, X., de Grijs, R., & Deng, L. 2015, Monthly Notices of the Royal Astronomical Society, 446, 1268, doi: [10.1093/mnras/stu2165](https://doi.org/10.1093/mnras/stu2165)
- Chen, X., de Grijs, R., & Deng, L. 2017, MNRAS, 464, 1119, doi: [10.1093/mnras/stw2390](https://doi.org/10.1093/mnras/stw2390)
- Chen, X., Wang, S., Deng, L., et al. 2019, Nature Astronomy, 3, 320, doi: [10.1038/s41550-018-0686-7](https://doi.org/10.1038/s41550-018-0686-7)
- Clark, J. S., Negueruela, I., Lohr, M. E., et al. 2015, Astronomy and Astrophysics, 584, L12, doi: [10.1051/0004-6361/201527360](https://doi.org/10.1051/0004-6361/201527360)
- Collaboration, G., Prusti, T., de Bruijne, J. H. J., et al. 2016, Astronomy and Astrophysics, 595, A1, doi: [10.1051/0004-6361/201629272](https://doi.org/10.1051/0004-6361/201629272)
- Collaboration, G., Vallenari, A., Brown, A. G. A., et al. 2023, Astronomy and Astrophysics, 674, A1, doi: [10.1051/0004-6361/202243940](https://doi.org/10.1051/0004-6361/202243940)
- Cruz Reyes, M., & Anderson, R. I. 2023, A&A, 672, A85, doi: [10.1051/0004-6361/202244775](https://doi.org/10.1051/0004-6361/202244775)
- De Somma, G., Marconi, M., Cassisi, S., et al. 2020, MNRAS, 496, 5039, doi: [10.1093/mnras/staa1834](https://doi.org/10.1093/mnras/staa1834)
- De Somma, G., Marconi, M., Molinaro, R., et al. 2022, ApJS, 262, 25, doi: [10.3847/1538-4365/ac7f3b](https://doi.org/10.3847/1538-4365/ac7f3b)
- Doig, P. 1925, The Observatory, 48, 112
- Feast, M. W., & Catchpole, R. M. 1997, MNRAS, 286, L1, doi: [10.1093/mnras/286.1.L1](https://doi.org/10.1093/mnras/286.1.L1)
- Freedman, W. L., Madore, B. F., Gibson, B. K., et al. 2001, The Astrophysical Journal, 553, 47, doi: [10.1086/320638](https://doi.org/10.1086/320638)

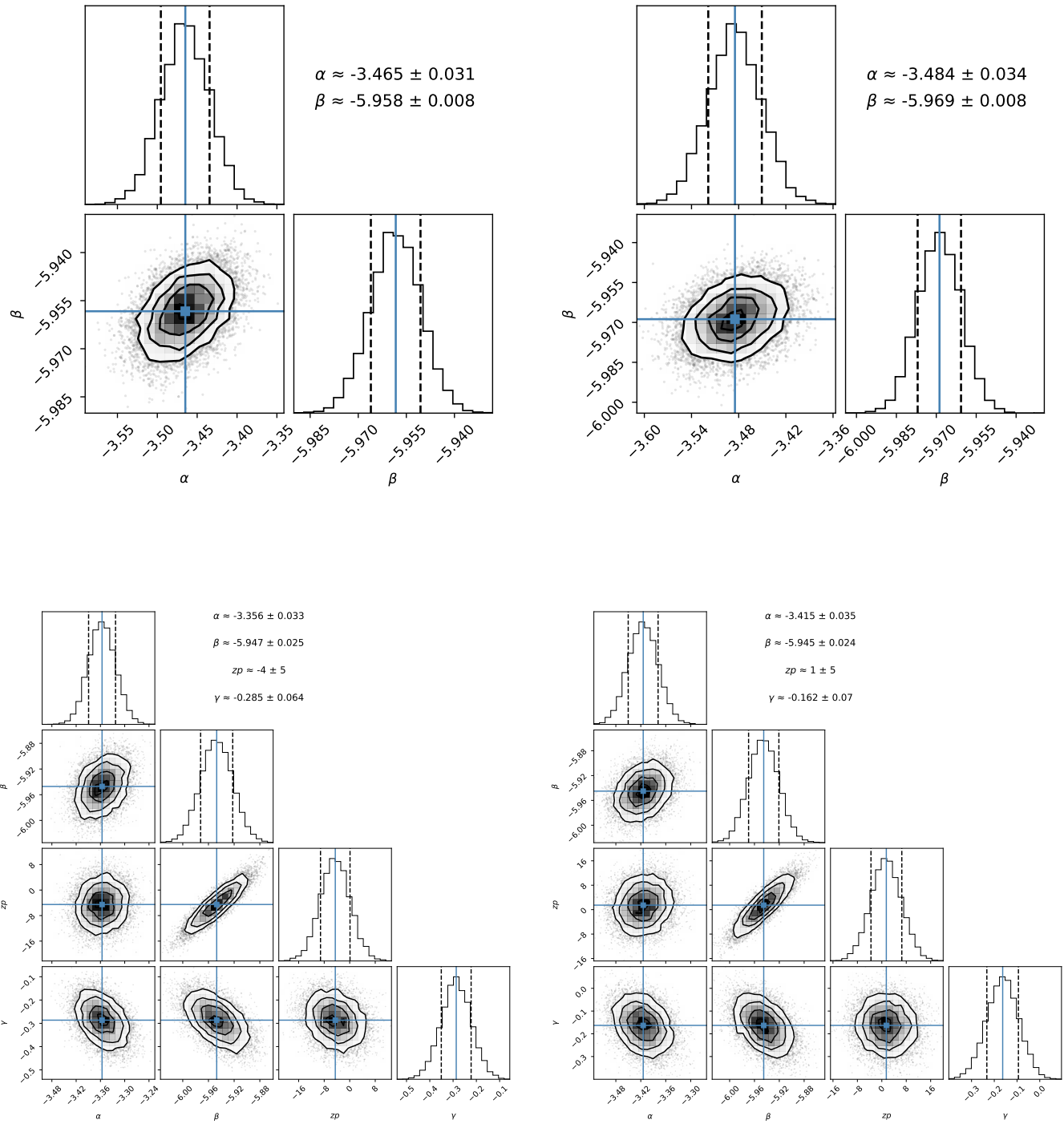


Figure C.1. The upper and lower corner plots represent the marginalised posterior distributions of the free parameters in PWR and PWZR, respectively. The vertical blue lines represent the median values, and the black dashed lines represent the 16th and 84th percentiles.

- Freedman, W. L., Madore, B. F., Scowcroft, V., et al. 2011, *The Astronomical Journal*, 142, 192, doi: [10.1088/0004-6256/142/6/192](https://doi.org/10.1088/0004-6256/142/6/192)
- Groenewegen, M. A. T. 2018, *A&A*, 619, A8, doi: [10.1051/0004-6361/201833478](https://doi.org/10.1051/0004-6361/201833478)
- Hao, C. J., Xu, Y., Wu, Z. Y., et al. 2022, *A&A*, 668, A13, doi: [10.1051/0004-6361/202244570](https://doi.org/10.1051/0004-6361/202244570)
- Hunt, E. L., & Reffert, S. 2023, *A&A*, 673, A114, doi: [10.1051/0004-6361/202346285](https://doi.org/10.1051/0004-6361/202346285)
- . 2024, *A&A*, 686, A42, doi: [10.1051/0004-6361/202348662](https://doi.org/10.1051/0004-6361/202348662)
- Kharchenko, N. V., Piskunov, A. E., Schilbach, E., Röser, S., & Scholz, R. D. 2013, *A&A*, 558, A53, doi: [10.1051/0004-6361/201322302](https://doi.org/10.1051/0004-6361/201322302)
- Leavitt, H. S., & Pickering, E. C. 1912, Harvard College Observatory Circular, 173, 1. <https://ui.adsabs.harvard.edu/abs/1912HarCi.173....1L>
- lin, Z., Xu, Y., Hao, C., et al. 2022, *ApJ*, 938, 33, doi: [10.3847/1538-4357/ac9051](https://doi.org/10.3847/1538-4357/ac9051)
- Lindgren, L., Bastian, U., Biermann, M., et al. 2021, *A&A*, 649, A4, doi: [10.1051/0004-6361/202039653](https://doi.org/10.1051/0004-6361/202039653)
- Lohr, M. E., Negueruela, I., Tabernero, H. M., et al. 2018, *Monthly Notices of the Royal Astronomical Society*, 478, 3825, doi: [10.1093/mnras/sty1280](https://doi.org/10.1093/mnras/sty1280)
- Madore, B. F. 1982, *The Astrophysical Journal*, 253, 575, doi: [10.1086/159659](https://doi.org/10.1086/159659)
- Maíz Apellániz, J., Pantaleoni González, M., & Barbá, R. H. 2021, *A&A*, 649, A13, doi: [10.1051/0004-6361/202140418](https://doi.org/10.1051/0004-6361/202140418)
- Majaess, D. J., Turner, D. G., & Lane, D. J. 2008, *Monthly Notices of the Royal Astronomical Society*, 390, 1539, doi: [10.1111/j.1365-2966.2008.13834.x](https://doi.org/10.1111/j.1365-2966.2008.13834.x)
- Marconi, M., Musella, I., & Fiorentino, G. 2005, *ApJ*, 632, 590, doi: [10.1086/432790](https://doi.org/10.1086/432790)
- Marconi, M., Musella, I., Fiorentino, G., et al. 2010, *ApJ*, 713, 615, doi: [10.1088/0004-637X/713/1/615](https://doi.org/10.1088/0004-637X/713/1/615)
- Medina, G. E., Lemasle, B., & Grebel, E. K. 2021, *MNRAS*, 505, 1342, doi: [10.1093/mnras/stab1267](https://doi.org/10.1093/mnras/stab1267)
- Molinaro, R., Ripepi, V., Marconi, M., et al. 2023, *MNRAS*, 520, 4154, doi: [10.1093/mnras/stad440](https://doi.org/10.1093/mnras/stad440)
- Negueruela, I., Dorda, R., & Marco, A. 2020, *Monthly Notices of the Royal Astronomical Society*, 494, 3028, doi: [10.1093/mnras/staa855](https://doi.org/10.1093/mnras/staa855)
- Pietrukowicz, P., Soszyński, I., & Udalski, A. 2021, *Acta Astronomica*, 71, 205, doi: [10.32023/0001-5237/71.3.2](https://doi.org/10.32023/0001-5237/71.3.2)
- Pietrzynski, G., Graczyk, D., Gallenne, A., et al. 2019, *Nature*, 567, 200, doi: [10.1038/s41586-019-0999-4](https://doi.org/10.1038/s41586-019-0999-4)
- Poggio, E., Drimmel, R., Cantat-Gaudin, T., et al. 2021, *A&A*, 651, A104, doi: [10.1051/0004-6361/202140687](https://doi.org/10.1051/0004-6361/202140687)
- Recio-Blanco, A., de Laverny, P., Palicio, P. A., et al. 2023, *A&A*, 674, A29, doi: [10.1051/0004-6361/202243750](https://doi.org/10.1051/0004-6361/202243750)
- Riess, A. G., Casertano, S., Yuan, W., et al. 2021, *The Astrophysical Journal*, 908, L6, doi: [10.3847/2041-8213/abdbaf](https://doi.org/10.3847/2041-8213/abdbaf)

- Riess, A. G., Breuval, L., Yuan, W., et al. 2022, *ApJ*, 938, 36, doi: [10.3847/1538-4357/ac8f24](https://doi.org/10.3847/1538-4357/ac8f24)
- Ripepi, V., Molinaro, R., Musella, I., et al. 2019, *A&A*, 625, A14, doi: [10.1051/0004-6361/201834506](https://doi.org/10.1051/0004-6361/201834506)
- Ripepi, V., Catanzaro, G., Molinaro, R., et al. 2020, *A&A*, 642, A230, doi: [10.1051/0004-6361/202038714](https://doi.org/10.1051/0004-6361/202038714)
- . 2021, *MNRAS*, 508, 4047, doi: [10.1093/mnras/stab2460](https://doi.org/10.1093/mnras/stab2460)
- Ripepi, V., Catanzaro, G., Clementini, G., et al. 2022, *A&A*, 659, A167, doi: [10.1051/0004-6361/202142649](https://doi.org/10.1051/0004-6361/202142649)
- Romaniello, M., Riess, A., Mancino, S., et al. 2022, *A&A*, 658, A29, doi: [10.1051/0004-6361/202142441](https://doi.org/10.1051/0004-6361/202142441)
- Sandage, A., & Tammann, G. A. 2006, *Annual Review of Astronomy and Astrophysics*, 44, 93, doi: [10.1146/annurev.astro.43.072103.150612](https://doi.org/10.1146/annurev.astro.43.072103.150612)
- Silverman, B. W. 1986, Density estimation for statistics and data analysis
- Skowron, D. M., Skowron, J., Mróz, P., et al. 2019, *Science*, 365, 478, doi: [10.1126/science.aau3181](https://doi.org/10.1126/science.aau3181)
- Trentin, E., Ripepi, V., Molinaro, R., et al. 2024, *A&A*, 681, A65, doi: [10.1051/0004-6361/202347195](https://doi.org/10.1051/0004-6361/202347195)
- Turner, D. G., Abdel-Sabour Abdel-Latif, M., & Berdnikov, L. N. 2006, *PASP*, 118, 410, doi: [10.1086/499501](https://doi.org/10.1086/499501)
- Udalski, A., Soszyński, I., Pietrukowicz, P., et al. 2018, *Acta Astronomica*, 68, 315, doi: [10.32023/0001-5237/68.4.1](https://doi.org/10.32023/0001-5237/68.4.1)
- Vasiliev, E., & Baumgardt, H. 2021, *MNRAS*, 505, 5978, doi: [10.1093/mnras/stab1475](https://doi.org/10.1093/mnras/stab1475)
- Zhou, X., & Chen, X. 2021, *Monthly Notices of the Royal Astronomical Society*, 504, 4768, doi: [10.1093/mnras/stab1209](https://doi.org/10.1093/mnras/stab1209)
- Zinn, J. C. 2021, *AJ*, 161, 214, doi: [10.3847/1538-3881/abe936](https://doi.org/10.3847/1538-3881/abe936)